Journal of Catalysis 456 (2026) 116770

Contents lists available at ScienceDirect

Journal of Catalysis

journal homepage: www.elsevier.com/locate/jcat

Research article

Electronic properties of PVA-PVAm ligands dictate mechanistic pathways in Au/AC-catalyzed HMF oxidation

Francesca Liuzzi [a,b], Stefano Scurti [a], Giacomo Fanciullo [a], Alessandro Allegri [a,b], Min Hu [c], Ivan Rivalta [a,b,d], Carmine D'Agostino [c,e], Atul Bansode [f], Daniele Caretti [a], Nikolaos Dimitratos [a,b], Stefania Albonetti [a,b,*]

[a] Industrial Chemistry "Toso Montanari" Department, University of Bologna, Via Piero Gobetti 85, Bologna 40129, Italy
[b] Center for Chemical Catalysis-C3, Alma Mater Studiorum Università di Bologna, Via Piero Gobetti 85, Bologna 40129, Italy
[c] Department of Chemical Engineering, The University of Manchester, Oxford Road, M13 9PL, UK
[d] ENSL, CNRS, Laboratoire de Chimie UMR 5182, 46 allée d'Italie, 69364 Lyon, France
[e] Dipartimento di Ingegneria Civile, Chimica, Ambientale e dei Materiali (DICAM), Alma Mater Studiorum – Università di Bologna, Via Terracini, 28, 40131 Bologna, Italy
[f] Department of Chemical Engineering, Delft University of Technology, Van der Maasweg 9, 2629 HZ Delft, the Netherlands

ARTICLE INFO

Keywords:
Stabilizer
Electronic effect
Gold colloidal nanoparticles
Heterogeneous catalysis
Biomass HMF oxidation

ABSTRACT

The development of efficient catalysts for the production of 2,5-furandicarboxylic acid (FDCA) from 5-(hydroxymethyl)furfural (HMF) is crucial to reduce the environmental footprint and achieve economically favorable conditions for its use in polyethylene 2,5-furandicarboxylate (PEF) synthesis. In this work, we demonstrated the possibility of tuning the electronic properties of Au nanoparticle-based catalysts via polymeric stabilizers to control HMF oxidation mechanism and product distribution. Polyvinyl alcohol (PVA), polyvinyl amine (PVAm), and poly(N-vinyl amine-co-vinyl alcohol) (PVA-co-PVAm) copolymers were synthesized with various compositions to evaluate the effect of functional groups on ligand–metal interactions. The presence of amino groups increases electron donation to Au, as confirmed by DFT calculations of monomer adsorption on cluster models of amorphous Au NPs. DFT investigations, NMR relaxation studies, and catalytic studies further revealed that increasing electron-donor groups modifies the reaction mechanism and enhances selectivity, particularly through manipulating the adsorption of reaction intermediates. These results provide mechanistic insights into the role of stabilizers and the active phase in directing specific reaction pathways. This understanding enables the rational design of polymeric ligands to enhance catalyst performance for aerobic oxidation of biomass-derived molecules in water under mild conditions, underscoring the role of stabilizer engineering in achieving selective and sustainable catalytic processes.

1. Introduction

Recently, the conversion and valorization of lignocellulosic biomass has been considered as one of the best alternatives to substitute traditional fossil-based feedstocks and produce valuable fuels and chemicals [1–5]. In particular, several studies have laid out a wide range of platform chemicals obtained through dehydration, hydrogenation, and/or oxidation reactions in separate or consecutive routes [6–10]. Among them, 2,5-furandicarboxylic acid (FDCA) produced from glucose/fructose dehydration, followed by 5-(hydroxymethyl)furfural (HMF) oxidation (Scheme 1) [11–15], is considered a potential bio-based alternative monomer to terephthalic acid, for the polymer industry [16,17].

Polyethylene 2,5-furandicarboxylate (PEF), for instance, is an excellent biopolymer substitute for polyethylene terephthalate (PET), which is obtained from fossil-based monomers [18]. Recent life cycle assessment (LCA) and techno-economic analysis (TEA) studies suggested that the production of HMF and FDCA-based products may offer lower impacts from CO_2 emissions than their fossil-based counterparts, but with an increase in environmental effects in other impact categories, such as high energy demands [19]. Recently, Avantium has brought FDCA production to a near-commercial scale, principally in response to

* Corresponding author.
E-mail address: stefania.albonetti@unibo.it (S. Albonetti).

https://doi.org/10.1016/j.jcat.2026.116770
Received 14 December 2025; Received in revised form 3 February 2026; Accepted 13 February 2026
Available online 16 February 2026

the interest shown by several global companies in using FDCA-based polymer in the manufacture of plastic drinks bottles [20–22]. Nevertheless, a deeper understanding of HMF oxidation reaction mechanism is needed, aiming for the design of more efficient catalytic systems, in making FDCA production economically favorable and at a lower environmental impact.

FDCA can be obtained through two oxidation pathways – alcohol oxidation and aldehyde oxidation, with alcohol oxidation being demonstrated to be the rate-determining step in the oxidation of HMF [23]. To promote HMF catalytic conversion, inorganic nanostructured materials based on mono- or bi-metallic nanoparticles (NPs) have emerged as suitable heterogeneous catalysts, [24–27] providing high-yielding routes to FDCA, while non-thermal catalytic methods, such as electro-[28–31] and photocatalytic [32–34] systems are also being recently considered as a way of further reducing energy requirements. Gold-based catalysts have been extensively investigated for the selective oxidation of HMF to FDCA [35–40]. In particular, when Au-based catalysts are employed, in order to promote the reaction, the presence of a homogeneous base is essential in amounts higher than the molar stoichiometric ratio [41]. The oxidation reaction mechanism of HMF has been investigated in depth. In particular, Davis et al. suggested a reaction mechanism in which H_2O inserts oxygen into the product and O_2 scavenges electrons from the metal catalyst [42].

Catalyst design was demonstrated to be crucial due to the strict correlation between active phase properties and the final mechanism observed [43,44]. Several synthetic methodologies to control and tune metal NPs properties have been investigated, among these, methods using preformed metal colloidal NPs represent one of the more flexible and simple approaches to synthesize well-designed NPs [45,46]. Usually, this technique involves the utilization of stabilizers during the colloidal preparation to prevent NPs aggregation and growth phenomena [47]. The stabilizing agent can significantly affect the catalytic performance of the final material; in fact, due to their electronic and steric properties, the activity and selectivity of the catalysts can be improved [48,49]. For this reason, tuning the properties of the capping ligand becomes a very important task during catalyst design, since it is possible to control the NPs' size and can have a pivotal role in the final catalytic activity [50]. Zhang et al. demonstrated the fundamental role of the capping ligand in the variation of the d-charge distribution of Au atoms [51]. For example, when a ligand that has a weak interaction with Au is used, the atoms in the NPs gain *5d* electrons, while those electrons are lost when thiol molecules with stronger interactions are used. The alteration of electronic density caused by the stabilizing agent can also enhance the catalytic performances of Au-based catalysts, as Tsukuda et al. observed [52].

In our previous works, [53–56] we have already demonstrated that the role of the stabilizing agent on Au NPs does not concern only the particle size control, but also affects the catalytic activity of the final material. In this study, we focus on the use of hydrosoluble polymeric stabilizers with different amounts of electron-donor groups on the macromolecular chain. Polyvinyl alcohol (PVA), polyvinyl amine (PVAm), and poly(vinyl alcohol)-poly(vinyl amine) (PVA-PVAm)-based copolymers were synthesized and employed as stabilizers during colloidal preparation of gold nanostructured heterogeneous catalysts, in order to evaluate how the presence of strong electron-donor groups (amino groups, as confirmed through DFT calculations) can influence the catalytic activity [57]. In particular, by tuning the electronic properties of the stabilizing agent, we observed significant changes in the product selectivity of cascade reactions, providing a design principle for better catalysts.

2. Experimental part

2.1. Materials

2-2′-Azo-bis-isobutyronitrile (AIBN), vinyl acetate (>99%), N-vinyl formamide (>99%), tetrachlorauric acid ($HAuCl_4{\cdot}3H_2O$), sodium borohydride ($NaBH_4$, 99%), activated carbon NORIT SX1G, sulfuric acid (H_2SO_4, 96%). HMF oxidation standards used for the (2,5-diformylfuran DFF, 5-hydroxymethyl-2-furan-carboxylic acid HMFCA, 5-formylfuran-2-carboxylic acid FFCA, 2,5-furandicarboxylic acid FDCA, and 2,5-bishydroxymethylfuran BHMF) were purchased from Toronto Research Chemicals), and 5-hydroxymethylfurfural was purchased from AVA Biochem (Zug, Switzerland). The polymeric stabilizers were properly synthesized following the methodologies described below. The solvents were used without further processes of purification.

2.2. Polymer preparation

Synthetic methodologies for the preparation of polymeric ligands, along with their spectroscopic and thermal characterizations, have been reported in the Supporting Information (SI).

2.3. Catalyst preparation

A colloidal gold solution was prepared by dissolving 0.76 g (1.9 mmol) of $HAuCl_4{\cdot}3H_2O$ in 200 mL of distilled H_2O. Then 5.5 mL were taken from the initial solution and diluted to 385 mL of distilled H_2O, to which was added a volume of 1% w/w polymer aqueous solution to obtain an Au:PVA weight ratio of 1:0.6. After 3 min, a freshly prepared aqueous solution of $NaBH_4$ (Au:$NaBH_4$ = 1:5 mol/mol) was added. A red Au^0 sol was immediately formed. The colloidal solution was stirred for 30 min, and, in the end, the Au colloidal NPs were immobilized by adding the activated carbon (AC) under vigorous stirring. The solution was acidified to pH 2 by using sulfuric acid. The amount of support was calculated to have a nominal metal loading of 1 wt%. The mixture was stirred for 1 h at room temperature. Then, the catalyst was filtered using a Buchner funnel and washed several times with distilled water to remove ionic species and mother liquors until a neutral pH was reached. After drying overnight at room temperature, the solids were dried at 80 °C in an oven for 4 h in static air conditions.

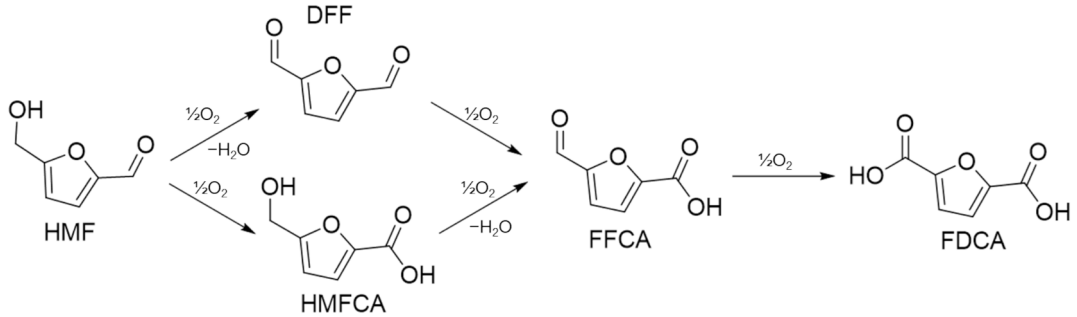

Scheme 1. Reaction pathways for HMF oxidation.

2.4. Characterization

The supported Au NPs were characterized by transmission electron microscopy (TEM) images and were obtained using a JEOL JEM-1400plus microscope to investigate the particle size and dispersion of the active phase. Samples were suspended in ethanol and treated by ultrasound for 15 min. A drop of the suspension was deposited on "quantifoil-carbon film" supported on a Cu grid and dried before analysis. TEM images were processed using ImageJ.

X-ray Photoelectron Spectroscopy (XPS) was conducted using a ThermoFisher K-α instrument to determine the oxidation state of the support material. Samples were prepared by placing powdered material onto carbon tape affixed to the sample holder, shaking off excess powder, and transferring the holder into the entry chamber. Once the pressure fell below 10^{-7} Pa, the sample was introduced into the analysis chamber, where the difference between the incident X-ray beam's fixed energy and the energy measured after reflection was used to determine the material's binding energy and oxidation state (range of 0 to 1400 eV). The X-ray photoelectron spectra obtained were analyzed using PHI SmartSoft (VersaProbe 4, Chanhassen, MN, USA) software and processed using the MultiPak 9.6.0.15 package. The binding energy values were referenced to the C1s signal at 284.5 eV. Shirley-type background and Gauss–Lorentz curves were used to determine the binding energies. Atomic concentration percentages of the characteristic elements were determined considering the corresponding area sensitivity factor for the different measured spectral regions.

2.5. Oxidation reactions

All the catalytic tests for the HMF oxidation were conducted in a 100 mL autoclave (Parr instrument). Standard reactions were performed using the following conditions: HMF:Au:NaOH molar ratios of 1:0.01:4 at 70 °C, 2 or 4 h of reaction time from the $t = 0$, the moment when the reaction temperature was reached, 10 bar of O_2, and 600 rpm stirring. After each reaction, the catalyst was separated from the reaction solution through centrifugation, and the solution was diluted with distilled water at a 1:5 vol/vol ratio to prepare the sample for the HPLC analysis. All the analyses were carried out in an Agilent 1260 Infinity instrument equipped with a BioRAD Aminex HPX-87H column and a DAD detector. To calculate the concentration of all species present in the reaction network (HMF, HMFCA, FFCA, BHMF, and FDCA), external calibration curves were utilized. Conversion, selectivity, and yield were calculated according to the following equations:

$$\text{Conversion}(\%) = \frac{[\text{HMF}]_0\text{-}[\text{HMF}]_F}{[\text{HMF}]_0} \times 100 \quad (1)$$

$$\text{Selectivity}\ (\%) = \frac{[\text{Product}]}{[\text{HMF}]_0\text{-}[\text{HMF}]_F} \times 100 \quad (2)$$

$$\text{Yield}\ (\%) = \frac{\text{Conversion} \times \text{Selectivity}}{100} \quad (3)$$

2.6. Computational details

The density functional theory (DFT) computational studies investigated the interaction of Au NPs with the stabilizers (PVA and PVAm), with the intermediates of the HMF oxidation reaction (DFF, HMFCA, FFCA), and with the probe molecules chosen for NMR studies (i.e., pentanal and pentanoic acid).

Gold nanoclusters, such as Au_{55}, have been successfully used as model systems for relatively small Au NPs, because their size lies in the regime where quantum effects, low-coordinated surface atoms, and structural disorder strongly influence their electronic properties, determining adsorption and reaction energetics [53,56]. Although smaller than the PVA(m)-stabilized Au NPs observed experimentally (3.3–5.1), the Au_{55} cluster (≈ 1 nm) provides a good compromise between computational cost and model reliability when treating this type of NPs at the *ab initio* level. In fact, at this level of theory, significantly larger clusters will be computationally too demanding, while periodic approaches (such as slab supercell models) are more appropriate for extended surfaces (typically present in NPs > 10 nm) and would capture less effectively the amorphous and undercoordinated surface structure of polymer-stabilized small NPs. Importantly, photoelectron spectroscopy combined with theoretical simulations has shown that anionic Au_n clusters in the size range $53 < n < 65$ do not adopt highly symmetric structures but instead exhibit distorted, amorphous-like structures [58]. Consistently, global structure optimizations performed at the DFT-B level identified the neutral amorphous Au_{55} cluster as a stable configuration [59]. While finite-size effects and the absence of support interactions represent inherent limitations of a Au_{55} cluster model of small Au NPS, the present study focuses on local adsorption motifs and relative energetics, for which cluster models have been shown to provide reliable mechanistic insight. In fact, this model has been successfully employed in previous theoretical studies to investigate adsorption, reaction intermediates, and interaction with polymer monomeric units [53,56], and we adopted the same approach here to ensure methodological consistency and mechanistic insight. To study the interaction of the PVA and PVAm stabilizers with the Au NPs, we considered as a representative model the adsorption of their monomers.

The adsorption energy ($\boldsymbol{E_{ads}}$) of each molecule (M) on the Au_{55} cluster model is computed as

$$\boldsymbol{E_{ads}} = \boldsymbol{E_{Au_{55}+M}} - \boldsymbol{E_{Au_{55}}} - \boldsymbol{E_M} \quad (4)$$

where $\boldsymbol{E_{Au_{55}+M}}$ is the ground-state (GS) energy of the Au_{55} + M complex, and $\boldsymbol{E_{Au_{55}}}$ and $\boldsymbol{E_M}$ are the GS energies of the isolated $Au_{55}$and M systems, respectively. The electron-donation extent between the PVA/PVAm monomers and Au_{55} has been calculated by determining the sum of the partial atomic charges on the Au_{55} and M moieties in the Au_{55} + M systems. All DFT calculations have been performed by using the B3LYP functional, [60] including the RI-J and COSX approximations [61] (with the def/J auxiliary basis set, [62] with solvent effect included also during geometry optimizations) using the polarizable continuum model [63] and the Becke-Johnson D3 corrections for dispersion interactions, [64] as implemented in the ORCA package [65]. For the Au atoms, the LANL2DZ basis set [66] along with the Hay-Wadt effective core potential [66] have been used. For the H, C, O, and N atoms, instead, the 6-31G** basis set has been employed for all geometry optimizations (see SI for the cartesian coordinates of the optimized Au_{55} + M systems), while adsorption energies have been obtained by refining the total energies with single-point calculations by using the larger 6–311++G** basis set. Corrections for the basis set superposition error have been introduced by considering the optimized geometries of isolated Au_{55} and M, which have been aligned to the geometries of the corresponding moieties in the optimized Au_{55} + M complex, thus with the basis set of Au_{55} (or M) in the Au_{55} + M complex being directly included in the energy of isolated M (or Au_{55}). For the partial atomic charges calculations, we computed both the atomic dipole corrected Hirshfeld [67] and the Merz-Kollman charges [68] methods by using the Multiwfn package [69].

2.7. NMR relaxation measurements

NMR relaxation measurements were performed on a Magritek SpinSolve benchtop spectrometer operating at a ^{1}H frequency of 43 MHz. The spin–lattice relaxation time (T_1) was measured using the inversion recovery sequence with a repetition time of $5 \times T_1$ [70]. Sixteen inversion delay times were used for each sample, and 32 scans were performed for each data point. The transverse relaxation time (T_2) was measured using the Carr-Purcell-Meiboom-Gill (CPMG) pulse sequence [71]. Catalyst samples were pretreated by soaking them in

pentanal or pentanoic acid as the chosen probe molecules for at least 48 h. Then samples were dried on a solvent-soaked filter paper to remove the excessive liquid on the external surface before transferring them to 5 mm NMR tubes. To minimize the effect of solvent evaporation, a small piece of pre-soaked filter paper was placed under the cap of the NMR tube. The tube was left in the magnet for around 15 min to achieve thermal equilibrium before the measurements.

3. Results and discussion

3.1. Computational results

This study aimed to demonstrate how the choice of polymeric stabilizer and its electronic properties influence the catalytic activity of gold nanoparticles, thereby affecting the reaction mechanism. With this goal, two different stabilizers were selected: polyvinyl alcohol (PVA) and polyvinylamine (PVAm). To better understand their interaction with the metal surface, DFT calculations were performed to determine the adsorption energies between the respective monomers and an Au_{55} cluster. These calculations were designed to provide evidence for the electron-donating capabilities of the stabilizers and how these characteristics might impact the electronic structure and catalytic behavior of the gold nanoparticles.

Fig. 1 shows the DFT optimized structures obtained for the PVA and PVAm monomers adsorbed on the Au_{55} cluster. We observed a smaller distance for the N-Au bond in the Au_{55} + PVAm complex (2.26 Å) with respect to the O-Au bond in the Au_{55} + PVA complex (2.49 Å), indicating a stronger interaction with Au NPs for the PVAm monomer. The difference in absorption geometries is associated with different adsorption energies, PVAm being more strongly bound to Au_{55} ($\boldsymbol{E_{ads}}$ = -25.2 kcal/mol) respect to PVA ($\boldsymbol{E_{ads}}$ = -11.6 kcal/mol). The 13.6 kcal/mol difference in adsorption energy is accompanied by a different electron-donation extent, computed as the difference in the sum of the partial atomic charges between the two moieties (the monomer and the Au_{55} cluster). Using the atomic dipole corrected Hirshfeld charges method to compute the partial charges, we observed that the negative charge injected in the Au_{55} moiety upon adsorption is smaller for the Au_{55} + PVA complex (−0.16 electrons) with respect to the Au_{55} + PVAm one (−0.33 electrons). Similar values have been obtained using the Merz-Kollman charges method (i.e., −0.13 and −0.37 electrons, respectively). These results indicate an enhanced monomer-to-Au_{55} electron-donation when PVA is replaced with PVAm, in line with the XPS analysis reported above.

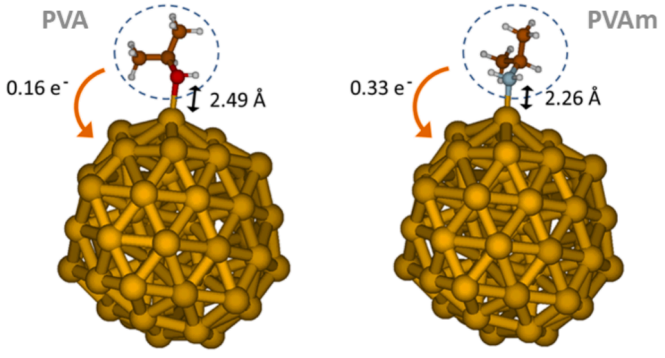

Fig. 1. The DFT optimized structures of monomers of the PVA (left) and the PVAm (right) stabilizing agents adsorbed on the Au_{55} cluster, modelling small Au NPs. The O-Au and N-Au equilibrium distances (in Å) and the stabilizer-to-NP electron-donation extent (using Hirshfeld charges) are also reported.

3.2. Synthesis and characterization of catalysts with different electron-donating groups

To evaluate the effect of different functional groups presented onto polymeric ligands on the catalytic mechanisms, poly(N-vinyl amine-co-vinyl alcohol) (PVA-co-PVAm) copolymers were synthesized by solution-free radical polymerization following the methodology described in the experimental section and subsequently hydrolyzed. The presence of amino groups on the macromolecules can alter the interaction between ligand and metal, due to the possible partial covalent bond formation between nitrogen and gold by π back-bonding of the metal on the empty π*-orbitals of the ligands, as demonstrated by DFT calculations before. Furthermore, this hypothesis can be confirmed following Hard-Soft Acid-Base (HSAB) theory, where primary amines are considered to have a borderline character between the hard and soft bases, and therefore their interaction with a soft acid center (Au NPs) can be explained by a bond with a partial covalent nature [72–75]. The real composition of the prepared copolymers in terms of the number of functional groups in the main chain (study reported in SI) represents crucial parameters to analyze the effect of polymeric ligands on the final catalytic materials. Employing these polymers, a series of Au-based catalysts was prepared via sol-immobilization method, [55,76] using activated carbon (AC) as the chosen support, and maintaining a polymer:Au weight ratio of 0.6 for the employed stabilizer in each NPs synthesis. In particular, two catalysts were prepared using the homopolymers PVA and PVAm (labelled Au/AC_PVA and Au/AC_PVAm), while for the others, copolymers with different PVAm:PVA composition were employed (the calculated PVAm molar percentage in the three copolymers is 16, 37, and 59).

All the prepared catalysts are reported in Table 1, and the samples stabilized with copolymers are denoted as Au/AC_PVAm_XX, where XX is the molar percentage of PVAm.

Each catalyst was characterized by TEM (Fig. 2) and XPS analysis to determine the mean particle size and particle size distribution of gold NPs, as well as the atomic percentage of gold on the catalyst surface and oxidation state of Au. TEM analysis (Table 1-S5, Fig. 2-S5) has shown that by increasing the amount of PVAm moieties, an increase in mean Au particle size from 3.3 to 5.1 nm can be observed. An increase in the nanoparticle's mean diameter can affect the activity of the catalyst. However, in a previous work, [53] we observed that in this range the mean particle size of Au is not the major factor for the observed catalytic performance, but the polymeric ligand can have an important effect in terms of catalytic activity. Furthermore, samples obtained from copolymers containing a higher number of amine moieties exhibited a broader particle size distribution of Au NPs, as indicated by observing the standard deviation of their particle size [77]. Overall, the use of a

Table 1
List of prepared catalysts along with their characteristics: percentage of PVA and PVAm in the stabilizing polymer, TEM NPs size, values of gold binding energy, and percentage of Au on the catalyst surface obtained from XPS analysis.

Catalyst	% PVAm*	% PVA	d_{TEM} (nm)	BE Au4f$_{7/2}$ (eV)	% Au on surface
Au/AC (No stabilizer)	–	–	7.9 ± 6.3	84.0	2.6
Au/AC_PVA	0	100	3.3 ± 0.7	84.0	1.6
Au/AC_PVAm_16	16	84	4.4 ± 1.3	84.1	0.9
Au/AC_PVAm_37	37	63	4.9 ± 0.9	84.1	0.9
Au/AC_PVAm_59	59	41	4.7 ± 1.3	83.9	2.0
Au/AC_PVAm	100	0	5.1 ± 1.4	83.7	1.2

*Copolymers' composition was calculated by integration of ^{1}H NMR spectra as described in SI.

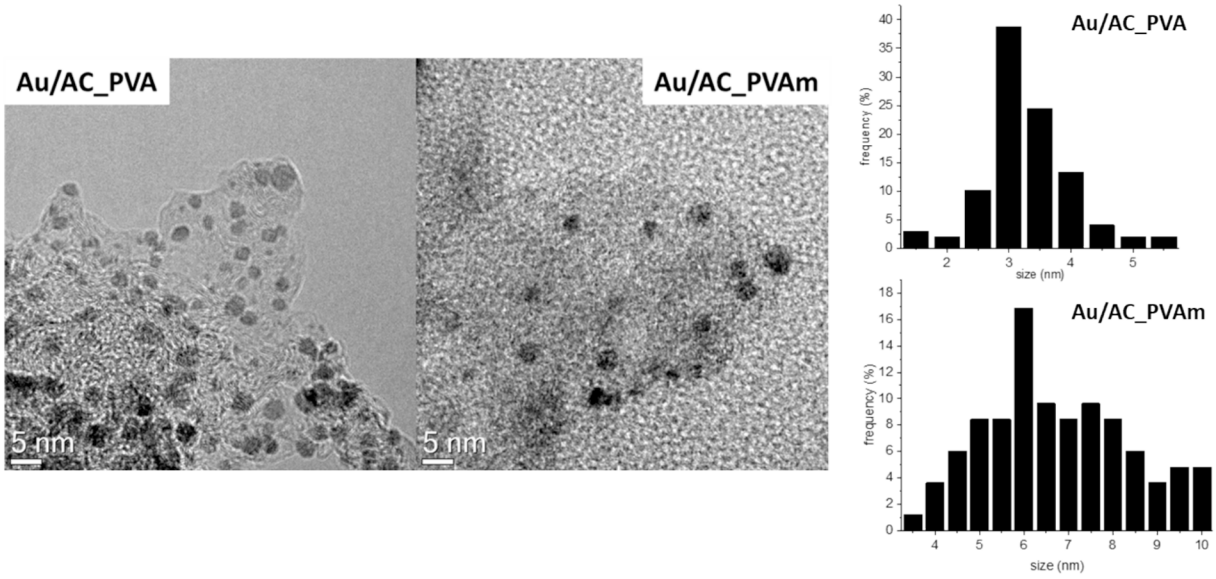

Fig. 2. TEM images and particle size distribution of the fresh catalyst Au/AC_PVA and Au/AC_PVAm.

polymeric resulted in catalysts with reduced average particle size diameters and lower dimension dispersions compared to the reference Au/AC catalyst that was prepared without a stabilizing agent.

XPS analysis showed the presence of metallic Au NPs. With the increase of PVAm, a decrease of BE was observed with the BE of Au4f$_{7/2}$ to shift from 84.1 to 83.7 eV, suggesting the presence of Au NPs with a partially negative charge (Au$^{\delta-}$) (Table 1 and S6, Fig. S7) [54]. The trend observed could be due to the electron-donor nature of amino groups, as previously reported for other polymers, such as PVP, which contains N atoms [78,79]. Typically, nitrogen-based ligands can interact with gold by partially covalent interaction due to the back-bonding mechanism between Au orbitals and nitrogen anti-bonding orbitals, which can suggest a modification of charge distribution in gold metal bonds [80–83]. Instead, the exposure of gold on the catalyst surface was varied from 1 to 2% without following a particular trend with respect to the amount of amines. Furthermore, a deconvoluted XPS spectroscopic signal related to N1s is reported in Fig. S8 with the aim of showing the presence of –NH$_2$ signals related to the polymeric ligands. In particular, the amount of amine peak decreases, in agreement with the composition calculated in Table S6.

3.3. NMR relaxation studies

The nature of these polymer stabilizers played a pivotal role in fine-tuning the surface properties of the catalysts, consequently influencing their interactions with reaction species.

NMR relaxation measurements were performed to probe surface interactions between the catalysts studied and the reaction species, using the T_1/T_2 ratio as an indicator of interaction strength [84–86]. Pentanal and pentanoic acid were used as model probe molecules to test the difference in behavior between an aldehyde and a carboxylic acid. It was not possible to use the actual reaction species for several reasons, most notably the fact that these species are solids at ambient conditions, hence they would not wet the catalyst pores and could not be measured effectively by NMR. Fig. 3 shows the NMR relaxation results of Au/AC_PVA and Au/AC_PVAm catalysts pretreated by pentanoic acid and pentanal, with the detailed information listed in Table S8. The data were fitted using the inversion recovery and CPMG exponential decay functions for T_1 and T_2, respectively (shown in Fig. S11).

When compared to the Au/AC_PVA catalyst, the Au/AC_PVAm catalyst exhibited a higher affinity towards pentanoic acid, the carboxylic acid, relative to pentanal, the aldehyde. Indeed, the T_1/T_2 ratio of

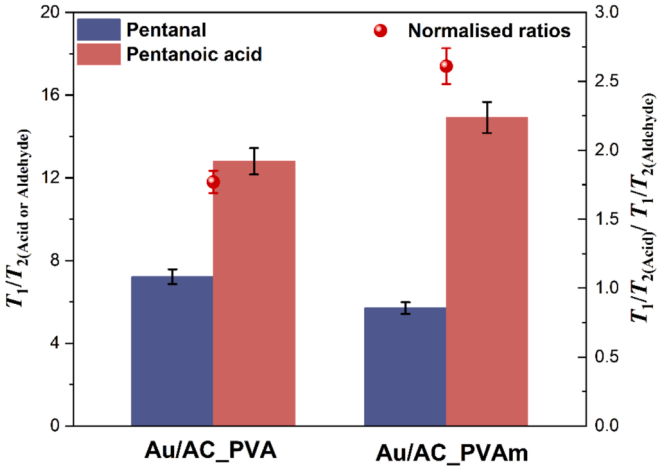

Fig. 3. NMR relaxation results with model probe molecules. Ratio of spin–lattice (T_1) and transverse (T_2) relaxation times of pentanal (blue bar), pentanoic acid (red bar), and normalized ratios of pentanoic acid over pentanal (red spheres). A higher T_1/T_2 ratio is associated with stronger surface affinity. (For interpretation of the references to colour in this figure legend, the reader is referred to the web version of this article.)

the acid normalized over that of the aldehyde was significantly higher for the Au/AC_PVAm when compared to Au/AC_PVA (see data represented by the red spheres in Fig. 3). This indicates a greater affinity of the acid compared to the aldehyde and can be rationalized by considering the enhanced interaction between the acid group of the carboxylic acid due to (i) the interaction between the amino groups from PVAm stabilizer and the acid groups as well as (ii) the charged surface of Au NPs of this catalyst. In the context of catalytic reactions, this interaction may be reducing or preventing the rapid desorption of the product from the catalyst surface. Moreover, the preferential interaction between the acid groups of the intermediates, such as HMFCA and FFCA, may alter the adsorption configuration of the intermediates, positioning the acid groups closer to the active sites while the aldehyde group remains further away, thereby inhibiting the aldehyde oxidation to the acid.

To support this hypothesis and complement the experimental data with structural insights, DFT adsorption studies on key HMF oxidation intermediates (DFF, HMFCA, and FFCA) were conducted, building on

the initial adsorption analysis of pentanal and pentanoic acid, used as NMR probes to reveal the preferential interaction of acid groups with Au NPs.

Fig. 4 shows the DFT optimized structures of pentanal and pentanoic acid (in both protonated and deprotonated forms) adsorbed on the Au_{55} cluster. Notably, if the pentanoic acid is protonated, adsorption is weaker than for pentanal, with E_{ads} of −15.2 and −17.4 kcal/mol, respectively, in contrast with experimental evidence that carboxylic acids bind Au more strongly than aldehydes. Upon deprotonation, however, pentanoic acid binds substantially more strongly than pentanal, with E_{ads} = –23.6 kcal/mol, in line with the NMR results. The adsorption geometries mirror these trends (see Fig. 4): pentanal forms a O–Au bond of 2.45 Å; the protonated acid binds monodentate with much longer O–Au distances (2.74 Å for the carbonyl O and 3.23 Å for the hydroxyl O); the deprotonated acid adopts a bidentate binding mode with short, nearly symmetric O–Au bonds (2.36–2.37 Å).

The good agreement between the computational and NMR results for the adsorption of pentanal and pentanoic acid prompted us to extend the DFT study to the adsorption of DFF, HMFCA, and FFCA, which are key intermediates in the HMF oxidation pathway. Based on the pentanoic acid results, which highlighted the critical role of deprotonation in strengthening adsorption, we restricted our analysis to the deprotonated forms of the carboxylic acids among these intermediates. This assumption is further supported by the basic experimental conditions of the HMF oxidation reaction, under which carboxylate species are expected to predominate.

Fig. 5 shows the optimized adsorption geometries of DFF, HMFCA, and FFCA intermediates. The DFF intermediate features two aldehydic groups directly linked to the furan ring, and it is found to bind the surface of the Au NP in a flat conformation. This binding mode, involving interaction between the furan ring and the Au surface, differs from that of pentanal (featuring only one aldehydic group that binds “on top” to an Au atom, see Fig. 4), having a slightly larger adsorption energy, with E_{ads} = -16.1 kcal/mol. In contrast, the HMFCA molecule, which features a carboxylic group and a hydroxymethyl (–CH_2OH) group linked to the furan ring, can make O-Au bonds with “on top” configuration with both the carboxylic and the hydroxymethyl group, due to the flexibility of the latter. The HMFCA binding mode features short O-Au distances of 2.34 and 2.51 Å for the carboxylic and the hydroxymethyl groups, respectively, (see Fig. 5) while maintaining a flat conformation and the furan-Au surface interaction, giving rise to an E_{ads} = -26.5 kcal/mol, larger than the bidentate pentanoic acid.

The FFCA intermediate, instead, features a carboxylic and an aldehydic group linked to the furan ring, binding to the Au NPs with one oxygen of its carboxylic group, in a monodentate fashion, as for HMFCA. This configuration maintains the furan-Au surface interaction and a flat conformation on the Au surface, but with the carbonyl group of the aldehydic moiety being far from surface Au atoms (O-Au equal to 3.42 Å). This binding mode, driven by the carboxylic group binding with a short O-Au distance (2.33 Å, similar to HMFCA), has an adsorption energy of −21.1 kcal/mol.

Thus, the DFT results clearly indicate that the strong interaction of carboxyl groups with the Au NPs determines larger adsorption energies for HMFCA and FFCA with respect to DFF, confirming that the preferential interactions of Au surface atoms with acid groups also occur in reaction intermediates. The binding modes observed for intermediates with aldehydic groups, i.e., DFF and FFCA, support the hypothesis of partial detachment from the Au surface (as they feature O-Au distances always larger than ca. 2.87 Å), eventually hindering their oxidation in the HMF conversion process on Au NPs.

3.4. Catalytic tests

3.4.1. Preliminary catalytic tests

All the prepared samples have been tested in the selective oxidation of 5-hydroxymethyl-2-furfural (HMF) to produce 2,5-furandicarboxylic acid (FDCA). The catalytic tests were performed using water as the solvent under the following reaction conditions: 70 °C, 10 bar of O_2, an HMF:Au:NaOH molar ratio of 1:0.01:4, and a stirring rate of 600 rpm.

To verify whether the optimized conditions from previous works are also optimal for these new catalytic systems, several studies have been conducted on the two catalysts prepared using the two homopolymers (Au/AC_PVA and Au/AC_PVAm).

First of all, a study to confirm that no external diffusional limitations are present was carried out, performing three tests at different stirring speeds using the Au/AC_PVA catalyst (Fig. S12). The results did not change when the stirring speed was set to 300 and 600 rpm. However, by decreasing the stirring speed to 150 rpm, the selectivity of the products changed, and a certain carbon loss could be observed. Probably, at such a low stirring speed, the diffusion of HMF to the active sites was not favored, and the reagent underwent degradation, leading to the formation of a significant amount of by-products (humins), in agreement with previous published reports [35,53]. The results obtained by varying the O_2 pressure (Fig. S13) in the range of 10–20 bar showed that the oxygen dissolved in water did not pose a limit for the reaction at these pressures; in fact, the values of HMF conversion and the product selectivity remained the same in each test. Furthermore, a study on the effect of reaction temperature was carried out using both catalysts prepared with homopolymers (Figs. S17 and S22). The results suggested that the desired reaction temperature to conduct the standard tests for the comparison of the catalysts was 70 °C, since the reaction was not complete at this temperature, and suitable selectivity in FDCA (which can be used as an indicator for comparing the catalytic activity) was observed (under 60% using the more active catalyst). Moreover, the effect of the

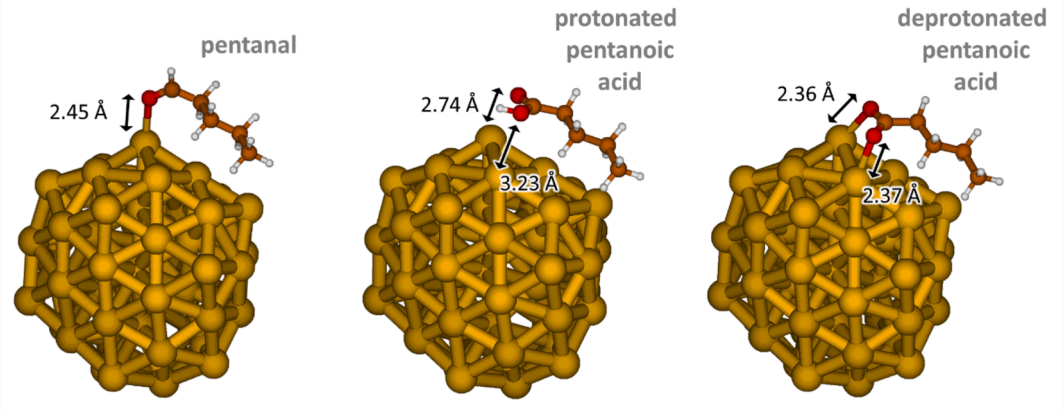

Fig. 4. The DFT optimized structures of pentanal (left), protonated (middle), and deprotonated (right) pentanoic acid adsorbed on the Au_{55} cluster, modelling small Au NPs. The O-Au binding distances (in Å) are also reported.

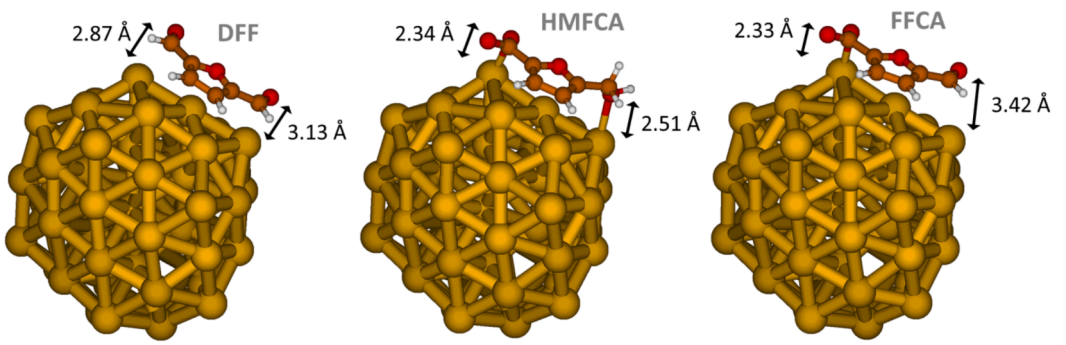

Fig. 5. The DFT optimized structures of DDF (left), HMFCA (middle), and FFCA (right) intermediates adsorbed on the Au_{55} cluster, modelling small Au NPs. The O-Au equilibrium distances (in Å) for the aldehyde, carboxyl, and hydroxyl groups are also reported.

NaOH concentration was evaluated for both catalysts (Figs. S15 and S20). This is a crucial factor for the reaction since a high concentration of a strong base can lead to the formation of by-products due to HMF degradation [41]. Variation of the NaOH:HMF molar ratio from 0 to 4 equivalents showed that the best results, in terms of selectivity of products and formation of by-products, were obtained when 4 equivalents of the base were employed. Since the aim of this work is to study the electronic effect of two different polymers, some tests were carried out by varying the quantity of the polymers during catalyst preparation (Figs. S14 and S19) and their molecular weight (Figs. S16 and S21) to exclude possible interferences related to these parameters. From the results presented in these studies, it was observed that using a polymer: Au weight ratio of 0.6 led to better catalytic results, while the molecular weight of the two polymers in the range considered (from 18,000 to 170,000 g/mol) did not affect the catalytic performances in a significant way. In fact, all catalysts showed a complete conversion of HMF, with the highest difference in the selectivity (~10%) of all the products. Finally, to confirm the effect of stabilizing agents on the catalytic performances of gold nanoparticles, a reference Au/AC catalyst synthesized in the absence of a stabilizer was evaluated. The results were compared with those obtained for the two catalysts prepared using the homopolymers (Fig. S28). A noticeable difference in product selectivity and distribution was observed, highlighting a significant influence of the stabilizing agents on the catalytic behavior.

3.4.2. *Investigation of the reaction mechanism*

To assess the influence of the electronic effects of the stabilizer, the catalytic performances of the prepared catalysts were evaluated in the selective HMF oxidation to FDCA at optimized reaction conditions. The results obtained are summarized in Table 2.

Focusing on the two catalysts stabilized with the homopolymers (PVA and PVAm), a significant difference was observed in product distribution and, therefore, selectivity. Increasing the percentage of PVAm, the conversion was always complete, while an increase in the selectivity to HMFCA was observed from 39% to 53%, whereas the selectivity to FDCA decreased from 61% to 12%. Moreover, when PVAm was the stabilizer, a certain quantity of FFCA was detected at the end of the reaction, and some by-products (probably humins) were formed, causing a loss in the overall carbon balance. Since a different selectivity trend in the final products was observed, to further investigate the possible causes, the catalytic performances of the two referenced catalysts (those with PVA and PVAm as Au stabilizers) were studied as a function of reaction time (Fig. 6). Concerning the PVA-based Au catalyst (Fig. 6A), it is notable that exclusively employing heat on the reaction mixture (time: 0 h) resulted in complete conversion of HMF, highlighting a pronounced catalytic activity. In particular, FDCA selectivity rapidly increased from 10% to 80% after 4 h of reaction. In the presence of the PVA-based Au catalyst and NaOH, HMF was rapidly oxidized to HMFCA, and its selectivity decreased along with the reaction time, while FDCA selectivity increased. FFCA was detectable in negligible quantities in all the tests due to the following reaction kinetics: FFCA formation is the rate-determining step of the reaction, while its oxidation is reasonably fast; for this reason, as soon as FFCA is produced it is further oxidized to FDCA in agreement with the literature [41]. From these results, it is evident that the reaction mechanism is coherent with those reported in the literature (Scheme 1) [36,43].

Table 2
Catalytic results of all the catalysts tested in HMF oxidation. Reaction conditions: 70 °C, 2 h, 10 bar O_2, HMF:Met:NaOH = 1:0.01:4.

Stabiliser	Conv. (%)	Selectivity (%) HMFCA	FFCA	FDCA	Others
PVA	>99	39	0	61	0
PVAm16	>99	59	1	29	11
PVAm37	>99	59	1	28	12
PVAm59	>99	52	10	16	22
PVAm	>99	53	11	12	24

Conversely, the catalytic results obtained for the PVAm-stabilized Au catalyst (Fig. 6B) showed a completely different catalytic behavior, which can be initially attributed to a catalyst with a different activity and, in particular, selectivity. The evolution of reaction products significantly changed when compared to the catalysts prepared using PVA to stabilize the Au-sol. HMF conversion was not completed after reaching the desired temperature (time 0 h), but only after 1 h of reaction. Selectivity to HMFCA gradually increased from 0 to 28%, while for FFCA, its selectivity gradually decreased. In particular, it is evident that in the presence of PVAm, the gradual increase in the selectivity of FDCA with the simultaneous decrease of selectivity to FFCA suggests that the former reacted to produce the desired dicarboxylic acid.

However, the absence of reactivity for HMFCA is evident in Fig. 6B, whereby the selectivity remained quite stable during reaction time, and no further conversion was observed. Probably, the reaction pathway involving this intermediate compound to FDCA formation does not occur, or the consecutive transformation has been blocked. To support this hypothesis, the reactivity of the reaction intermediates has been studied. Moreover, it is noted that during all the catalytic tests, there was always a certain amount of by-products. This can also highlight the different activity of this catalyst compared to the one stabilized with PVA. Under such basic reaction conditions, HMF can easily degrade to humins that cannot be quantified if it is not further converted into the other products [87]. The observed decrease of the by-products as the reaction progresses can be attributed to the equilibrium between the HMF and the first products that lead to the formation of humins, [88] to a strong interaction between the products and the catalyst, or to the formation of an unidentified product.

These results suggest that the reaction pathway has probably been altered compared with the scheme previously reported (Scheme 1). Similar results that suggest a modification in reaction mechanism were

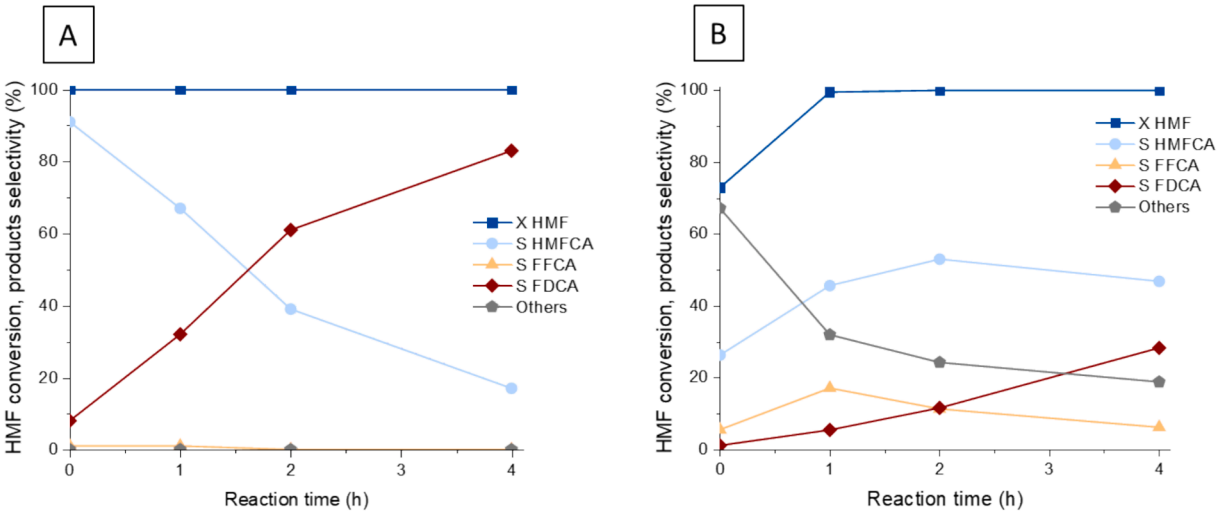

Fig. 6. HMF conversion (X) and products selectivity (S) as a function of reaction time for the catalyst prepared employing Au the NPs stabilized with PVA (A) and PVAm (B). Reaction conditions: 70 °C, 10 bar O_2, HMF:Met:NaOH = 1:0.01:4.

already observed previously on a bimetallic Pd_1Au_6–TiO_2 catalyst calcined at 300 °C [89]. However, according to the best of our knowledge, it has never been reported that the reaction pathway can be altered to control product selectivity by varying the nature of the stabilizer.

To further investigate and prove the existence of an alternative reaction pathway, some of the reaction intermediates were tested as starting reagents for further understanding of the reaction pathway. In previous studies, we have reported that the calcination treatment on Pd_1Au_6–TiO_2 altered to a certain degree the active surface phase, and a reaction mechanism for the FDCA formation from HMF was proposed, which is shown in Scheme 2. In order to demonstrate that the presence of PVAm as a stabilizer altered the reaction pathways, several tests using the intermediates as reagents were carried out. The reference catalyst was the Au/AC_PVAm (with 100% PVAm). The results obtained from these tests are shown in Table S8. Moreover, the same tests were carried out using the Au/AC_PVA to obtain a clear comparison with the Au/AC_PVAm results (Table S9).

Firstly, we investigated the presence or absence of the base-induced Cannizzaro reaction of HMF (Fig. S31 and Reaction (2) to HMFCA and 2,5-bishydroxymethylfuran (BHMF), carrying out the HMF reaction in the presence of N_2; using the same reaction conditions we used in the presence of O_2. The results (Table S9, Entry 1) confirmed the absence of the base-induced Cannizzaro reaction under N_2 atmosphere; indeed, at the end of the reaction, there was no presence of HMFCA and BHMF, which are the main products in the case of base-induced Cannizzaro reaction between HMF molecules [89]. When the same reaction was conducted under 10 bar of O_2 (Table S9, Entry 2) the formation of HMFCA and FFCA could be observed. These results prove that HMFCA (Scheme 2, pathway 1) and FFCA were formed due to the HMF oxidation. After these tests on the HMF, HMFCA, which is one of the first reaction intermediates, was used as a reagent to conduct a catalytic test. The catalytic results of this test (Table S9, Entry 3) showed the inability of Au/AC_PVAm to activate HMFCA, a low conversion of that molecule was observed, and only a 3% yield of FFCA was obtained. Using this catalyst, only the first step of the reaction (1) reported in Scheme 2 (in blue) could be achieved, while the oxidation of HMFCA to FFCA could not occur. Another important reaction intermediate to test as a reagent is DFF, since the alternative reaction pathway (green color pathway shown in Scheme 2) for the formation of FFCA and FDCA can be via the DFF formation and its consecutive oxidation (reaction pathway 2). Using DFF as a reagent, under O_2 (Table S9, Entry 4), it is evident that the molecule was easily oxidized to FFCA (65% of yield), but only a negligible amount

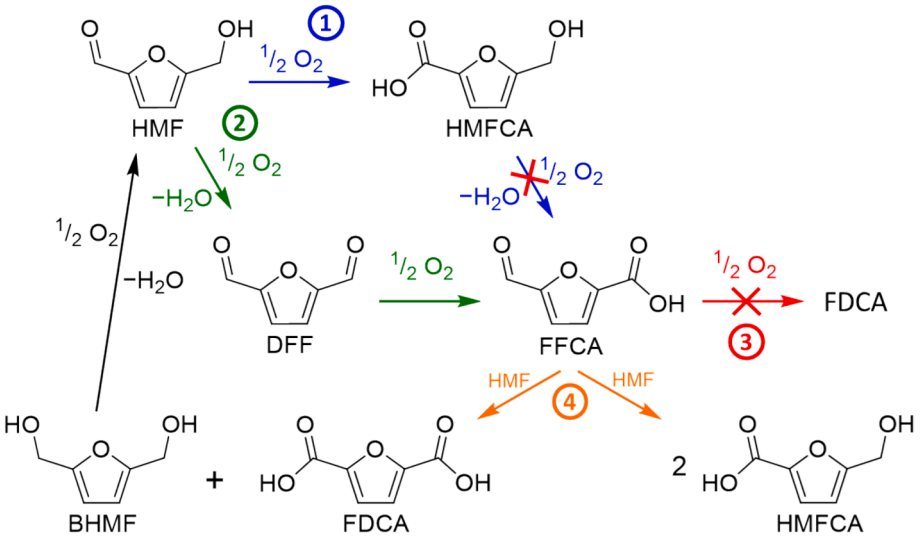

Scheme 2. Reaction pathways for HMF oxidation on Au/AC_PVAm catalyst.

of FDCA was detected (2% yield). This confirms that the formation of FFCA in the reaction environment can follow this reaction pathway (reaction pathway 2 in green color, Scheme 2), even if DFF was never detected in our tests. However, when the same test was conducted using N_2 pressure (Table S9 Entry 6), the molecule did not react with itself in a Cannizzaro reaction scenario. These results highlight a clear difference from the previous work, [89] in particular, it was confirmed that Cannizzaro disproportionation contributed to DFF conversion, forming HMF and FFCA, as products of the Cannizzaro reaction of DFF (Fig. S31, Reaction (4).

From our tests, it appears that DFF degradation prevailed over disproportionation, even if we used 2 mol of base with respect to the reagent (Table S9, Entry 5), to reproduce the same reaction conditions of the previous work. At this point, the results demonstrate that FFCA was mainly formed through DFF oxidation, but it seems that this molecule could not be further oxidized to produce FDCA. Indeed, when FFCA was used as a starting reagent (Table S9, Entry 7), a conversion higher than 40% was observed, but only an FDCA yield of 5% was achieved. Performing the same catalytic test under an inert atmosphere (Table S9, Entry 9) allows obtaining a higher conversion (98%), leading to a significant formation of byproducts (90%) and the same amount of FDCA, while without the presence of the catalyst, no conversion was observed (Table S9, Entry 8). Probably the presence of the catalyst facilitated the activation of the Cannizzaro reaction of FFCA with itself in a small percentage, and also the degradation of FFCA, explaining the high conversions of the reagent observed in the presence of N_2. However, the FFCA oxidation could not happen (pathway 3 in red, Scheme 2). To understand if the FDCA was formed from the Cannizzaro reaction between HMF and FFCA, a test using FFCA and HMF as reagents, in a molar ratio of 1:1, was done, and the formation of HMFCA and FDCA (Table S9, Entry 10) was observed. Most likely, during the HMF oxidation, FFCA formed through the DFF oxidation could react with the residual reagent HMF (reaction pathway 4, in orange color, Scheme 2) through a Cannizzaro-type reaction, yielding three different products in two scenarios. The first one is the formation of one molecule of BHMF and one of FDCA, and the second one is the formation of two molecules of HMFCA. The formed BHMF was rapidly oxidized to HMF as shown in Table S9, Entry 11.

In order to confirm the fundamental difference in the reaction mechanism, some of the most essential tests on the reaction intermediates have also been conducted using the catalyst Au/AC-PVA (Table S10), and two main differences could be observed. Firstly, HMFCA was still slowly oxidized to FFCA (this second step is usually the rate-determining step of the reaction [41]). In fact, the conversion was only 13% (Table S10, Entry 1), but as soon as the second compound was formed, it was rapidly oxidized to FDCA (10% yield). Secondly, when FFCA was used as a reactant (Table S10, Entry 3), after 30 min of reaction, it was almost completely converted into FDCA (95% yield). The obtained results demonstrate that the presence of PVAm to stabilize the gold NPs altered the reaction mechanism for the FDCA formation. The amino groups on PVAm are stronger electron donors than the –OH of PVA, which can alter the surface electron density on Au NPs, partially charging it and probably causing the modification of the mechanism. As suggested by the DFT calculations, the strong affinity of the intermediates HMFCA and FFCA, arising from the presence of the carboxylic acid group, may hinder the overall HMF oxidation process. This effect appears particularly pronounced for the catalyst stabilized with PVAm, which exhibits an even stronger interaction with carboxylic acid functionalities, as demonstrated by the NMR relaxation studies. Therefore, Davis et al. demonstrated that HMF oxidation was promoted by the presence of hydroxide ions in water, facilitating the activation of the alcoholic group of HMF or adding to the aldehyde during their oxidation to acid products [42, [39]. In this case, the gold role is to accept electrons during the oxidation of the substrates, while molecular oxygen acts as an electron scavenger from the nanoparticle's surface to close the catalytic cycle (Fig. S30). Thus, the ability of Au to accept and release electrons profoundly affects catalytic activity, and therefore, the presence of stabilizers with peculiar electronic features can play a direct role. In this case, the amino groups of PVAm modify the partial surface charge of gold, as is evident by XPS analysis and computational studies, and therefore alter the reaction mechanism and inhibit the Au role as electron acceptors, in addition to the molecules' adsorption on the catalyst surface. In the majority of cases, the catalytic behavior of colloidal Au-based catalysts is closely related to the presence of Au NPs in a metallic state in the absence or presence of a negative charge, and therefore, the capability of Au NPs to accept electrons during the selective oxidation of the organic substrates. The metal–ligand interphase of the supported Au colloidal nanoparticle can promote the activation of the adsorbed reactant and intermediates and consequently determine not only activity but also selectivity to the desired products. Therefore, the electronic properties of Au have been further tuned through the employment of copolymers with different compositions of the amino group bearing the same two functionalities (–OH and $–NH_2$) previously studied. Three catalysts with different percentages of amino groups were prepared using the copolymers as stabilizers (Table 1), and the catalytic performance for HMF oxidation was evaluated at the same reaction conditions.

In Fig. 7 the results obtained from the catalytic tests of the catalysts as a function of the percentage of PVAm are summarized.

The HMF conversion was always 100%; for this reason, it is not reported in the graph (Fig. 7). Comparing the selectivity of products, the Au catalyst with the best catalytic performance was obtained when PVA was chosen as the stabilizer, showing a FDCA selectivity of more than 60%. Increasing the amount of amino groups as polymer functionalities, the activity of the catalysts began to decrease. When the percentage of $–NH_2$ is 16% and 37%, the FDCA selectivity remained under 30%, and the by-products formation in the reaction environment became relevant, suggesting inhibition in the formation of FDCA and alteration of reaction pathways with an increase in by-products. The decrease in the catalytic performance observed further increased when the percentage of amino groups prevailed. The selectivity of FDCA decreased below 20%, while the by-product amount increased significantly. Moreover, a significant amount of FFCA was formed after 2 h of reaction, suggesting that its oxidation, which is usually a fast step of the reaction, was not favored on this catalyst [41]. Some tests performed using HMFCA and FFCA as reagents were carried out on the two catalysts Au/AC_PVAm16 and Au/AC_PVAm59. Catalytic data from these studies (Table S11) indicate that the variation in the reaction mechanism had already begun when the

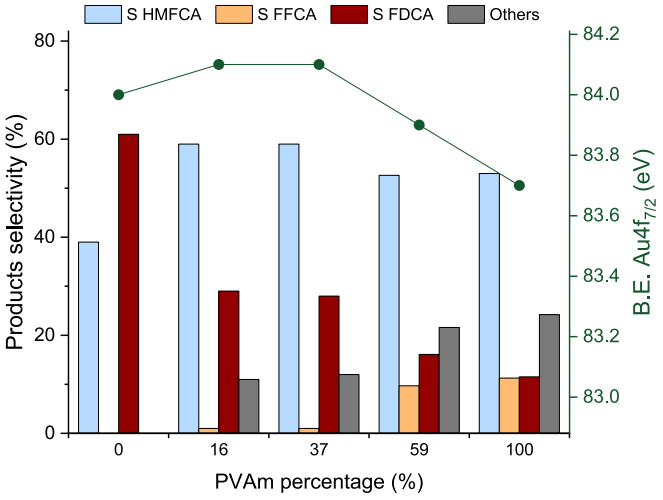

Fig. 7. Catalytic performance of Au catalysts as a function of stabilizer composition, and comparison of the obtained results with the binding energy of the Au $4f_{7/2}$ peak by XPS analysis. HMF conversion is complete in each test. Reaction conditions: 70 °C, 2 h, 10 bar O_2, HMF:Met:NaOH = 1:0.01:4. S represents the selectivity.

amount of amino groups exceeded 50%. However, the catalyst with 100% PVAm as stabilizer was the one that showed the lowest activity, presenting a higher amount of by-products and a lower FDCA selectivity (12%), suggesting the complete alteration of the reaction pathway for FDCA formation and therefore the inhibition of the consecutive oxidation.

The catalytic activity as a function of the quantity of amino groups on the macromolecular chain follows a trend in line with the shift towards lower binding energy highlighted in XPS analysis. This can confirm that the alteration of the Au-Au bond in terms of a change of charge density due to the electron-donor nature of amino groups is the cause of the reactivity variation and therefore of the catalytic mechanism. In this way, we have demonstrated the active role of polymeric stabilizers characterized by the presence of electron-donor groups ($–NH_2$) in the side chain in the HMF selective oxidation reaction. In particular, their employment not only modified the surface electronic properties of gold nano-catalysts but also altered the catalytic route, and therefore, it affected the reaction mechanism. To conclude the investigation of the stabilizer effect, the catalyst's stability was investigated. Particularly, four catalysts were examined: two prepared using the homopolymers (PVA and PVAm) and two prepared using copolymers containing the highest and lowest percentage of $–NH_2$ groups. Each catalyst was tested in three consecutive reaction cycles (Figs. S18, S23, S25, and S27). Three samples, Au/AC_PVA, Au/AC_PVAm16, and Au/AC_PVAm59, exhibited similar behaviour: a decrease in catalytic activity after the second reaction cycle was observed, consistent with the results reported in the literature on the low stability of gold NPs for the HMF oxidation reaction [36,41]. Notably, the activity loss observed for the PVA-based catalyst was slower than that of the two copolymer-stabilized catalysts. Indeed, after the third reaction cycle, these two catalysts exhibited an amount of by-products higher than 50%, whereas the PVA-stabilized catalyst only produced a 5% of by-products. On the other hand, the activity of the PVAm-stabilized catalyst displayed a different behaviour. The loss of activity after the first use resulted in a higher selectivity of HMFCA, accompanied by a decrease in the quantity of other products. The same product distribution was maintained after the third reaction. To gain further insight into the catalyst deactivation observed during the reusability tests, XPS and TEM analyses were performed on the spent catalysts (Table S7, Figs. S9 and S10). TEM images revealed a marked loss of nanoparticle dispersion on the support, accompanied by pronounced particle aggregation on the catalyst surface. This trend was in accordance with XPS measurements, which showed a significant decrease in the surface Au content compared to the fresh catalysts. Together, these findings suggest that weak metal–support interactions, combined with the relatively high reaction temperature, promote nanoparticles' mobility on the catalyst surface, leading to coalescence and deactivation [90,91].

4. Conclusions

The electronic effect of different stabilizers, two homopolymers (PVA and PVAm), and three copolymers, was investigated for the preparation of Au-based catalysts for the 5-hydroxymethylfurfural (HMF) oxidation. By varying the amount of electron donor group on the stabilizer, changes in the reaction mechanism and distribution of products were observed. DFT studies of monomers' adsorption on an Au_{55} cluster model, along with XPS analysis, confirmed that amino groups alter the surface charge density, thereby modulating catalyst reactivity. NMR relaxation studies performed using pentanal and pentanoic acid as model probe molecules further clarified these observations, revealing a stronger affinity of carboxylic acid groups compared to aldehyde groups, especially when PVAm was employed as the stabilizer. The enhanced interaction of the carboxylic acid groups was supported by DFT on the model molecules and reaction intermediates. Furthermore, systematic catalytic studies using the different intermediates as reagents enabled elucidation of the new reaction network. The outcome of this research is to emphasize the importance of considering the electronic properties of the stabilizing agent, and of the catalyst in general, to tune the product distribution for the HMF oxidation. The present study can be used as an example for a range of important biomass-derived platform chemicals for oxidation or hydrogenation processes.

Author contributions

Nikolaos Dimitratos, Stefania Albonetti, and Daniele Caretti supervised the project and designed the experiments, Francesca Liuzzi, Stefano Scurti, and Alessandro Allegri carried out the synthesis of materials and catalytic testing; Ivan Rivalta and Giacomo Fanciullo carried out the computational studies and interpreted the data; Carmine D'Agostino and Min Hu carried out the NMR relaxation studies and interpreted the data; Nikolaos Dimitratos, Stefania Albonetti, Carmine D'Agostino, Ivan Rivalta, Daniele Caretti Francesca Liuzzi, Stefano Scurti, Min Hu, Giacomo Fanciullo, and Alessandro Allegri were involved in the writing and editing of the manuscript.

CRediT authorship contribution statement

Francesca Liuzzi: Writing – review & editing, Writing – original draft, Validation, Methodology, Investigation, Formal analysis. **Stefano Scurti:** Writing – review & editing, Validation, Investigation, Formal analysis, Data curation. **Giacomo Fanciullo:** Writing – review & editing, Validation, Methodology, Investigation, Formal analysis, Data curation. **Alessandro Allegri:** Writing – review & editing, Validation, Data curation. **Min Hu:** Writing – review & editing, Methodology, Investigation, Formal analysis, Data curation. **Ivan Rivalta:** Writing – review & editing, Supervision, Software, Resources, Methodology, Formal analysis, Data curation. **Carmine D'Agostino:** Writing – review & editing, Supervision, Resources, Methodology, Formal analysis, Data curation. **Atul Bansode:** Writing – review & editing, Resources, Investigation. **Daniele Caretti:** Writing – review & editing, Supervision, Resources, Methodology, Investigation, Data curation. **Nikolaos Dimitratos:** Writing – review & editing, Writing – original draft, Visualization, Supervision, Methodology, Investigation, Conceptualization. **Stefania Albonetti:** Writing – review & editing, Writing – original draft, Visualization, Supervision, Resources, Project administration, Methodology, Investigation, Funding acquisition, Conceptualization.

Declaration of competing interest

The authors declare that they have no known competing financial interests or personal relationships that could have appeared to influence the work reported in this paper.

Acknowledgements

M. H. and C. D. would like to acknowledge the EPSRC (EP/V026089/1) for supporting their research activities. I. R. gratefully acknowledges the use of HPC resources of the "Pôle Scientifique de Modélisation Numérique" (PSMN) of the ENS-Lyon, France. AA acknowledges a research contract funded by an FSE + 2021–2027 grant according to art. 24, comma 3, lett. a), Legge 240/2010 e s.m.i. e del D. G.R. 693/2023 (2023-20090/RER-6 - CUP: J19J23000730002). SS acknowledges a research contract funded by FSE + 2021–2027 grant according to art. 24, comma 3, lett. a), Legge 240/2010 e s.m.i. e del D.G. R. 693/2023 (2023–20090/RER-2-CUP: J19J23000730002). Authors wish to acknowledge Mr. Bart Boshuizen for the XPS analysis.

Appendix A. Supplementary data

Supplementary data to this article can be found online at https://doi.org/10.1016/j.jcat.2026.116770.

Data availability

Data will be made available on request.

References

[1] R.A. Sheldon, Green and sustainable manufacture of chemicals from biomass: state of the art, Green Chem. 14 (2014).
[2] D.M. Alonso, J.Q. Bond, J.A. Dumesic, Catalytic conversion of biomass to biofuels, Green Chem. 12 (2010) 1493–1513, https://doi.org/10.1039/C004654J.
[3] J.N. Chheda, G.W. Huber, J.A. Dumesic, Liquid-phase Catalytic Processing of Biomass-Derived Oxygenated Hydrocarbons to Fuels and Chemicals, Angew. Chem. Int. Ed. 46 (2007) 7164–7183, https://doi.org/10.1002/anie.200604274.
[4] L. Wu, T. Moteki, A.A. Gokhale, D.W. Flaherty, F.D. Toste, Production of Fuels and Chemicals from Biomass: condensation Reactions and beyond, Chem 1 (2016) 32–58, https://doi.org/10.1016/j.chempr.2016.05.002.
[5] G. Fiorentino, M. Ripa, S. Ulgiati, Chemicals from biomass: technological versus environmental feasibility. a review, Biofuels Bioprod. Biorefining 11 (2017) 195–214, https://doi.org/10.1002/bbb.1729.
[6] T. Werpy, G. Petersen, Top Value Added Chemicals from Biomass: Volume I – Results of Screening for Potential Candidates from Sugars and Synthesis Gas, 2004. DOI: 10.2172/15008859.
[7] Z. Jiang, Y. Zeng, D. Hu, R. Guo, K. Yan, R. Luque, Chemical transformations of 5-hydroxymethylfurfural into highly added value products: present and future, Green Chem. 25 (2023) 871–892, https://doi.org/10.1039/D2GC03444A.
[8] G. Sanghez de Luna, P.H. Ho, A. Sacco, S. Hernández, J.-J. Velasco-Vélez, F. Ospitali, A. Paglianti, S. Albonetti, G. Fornasari, P. Benito, AgCu Bimetallic Electrocatalysts for the Reduction of Biomass-Derived Compounds, ACS Appl. Mater. Interfaces 13 (2021) 23675–23688, https://doi.org/10.1021/acsami.1c02896.
[9] D.A. Giannakoudakis, V. Nair, A. Khan, E.A. Deliyanni, J.C. Colmenares, K. S. Triantafyllidis, Additive-free photo-assisted selective partial oxidation at ambient conditions of 5-hydroxymethylfurfural by manganese (IV) oxide nanorods, Appl. Catal. B Environ. 256 (2019) 117803, https://doi.org/10.1016/j.apcatb.2019.117803.
[10] M. Annatelli, J.E. Sánchez-Velandia, G. Mazzi, S.V. Pandeirada, D. Giannakoudakis, S. Rautiainen, A. Esposito, S. Thiyagarajan, A. Richel, K. S. Triantafyllidis, T. Robert, N. Guigo, A.F. Sousa, E. García-Verdugo, F. Aricò, Beyond 2,5-furandicarboxylic acid: *status quo* , environmental assessment, and blind spots of furanic monomers for bio-based polymer, Green Chem. (2024), https://doi.org/10.1039/D4GC00784K.
[11] H. Kim, J. Kim, W. Won, Toward Economical and Sustainable production of Renewable Plastic: integrative System-Level analyses, ChemSusChem 15 (2022) e202200240, https://doi.org/10.1002/cssc.202200240.
[12] G. Totaro, L. Sisti, P. Marchese, M. Colonna, A. Romano, C. Gioia, M. Vannini, A. Celli, Current advances in the Sustainable Conversion of 5-Hydroxymethylfurfural into 2,5-Furandicarboxylic Acid, ChemSusChem 15 (2022) e202200501, https://doi.org/10.1002/cssc.202200501.
[13] Z. Zhang, G.W. Huber, Catalytic oxidation of carbohydrates into organic acids and furan chemicals, Chem. Soc. Rev. 47 (2018) 1351–1390, https://doi.org/10.1039/C7CS00213K.
[14] P. Pal, S. Saravanamurugan, Recent advances in the Development of 5-Hydroxymethylfurfural Oxidation with Base (Nonprecious)-Metal-Containing Catalysts, ChemSusChem 12 (2019) 145–163, https://doi.org/10.1002/cssc.201801744.
[15] R. Wojcieszak, I. Itabaiana, Engineering the future: perspectives in the 2,5-furandicarboxylic acid synthesis, Catal. Today 354 (2020) 211–217, https://doi.org/10.1016/j.cattod.2019.05.071.
[16] A. Gandini, The irruption of polymers from renewable resources on the scene of macromolecular science and technology, Green Chem. 13 (2011) 1061–1083, https://doi.org/10.1039/C0GC00789G.
[17] C. Moreau, M.N. Belgacem, A. Gandini, Recent Catalytic advances in the Chemistry of Substituted Furans from Carbohydrates and in the Ensuing Polymers, Top. Catal. 27 (2004) 11–30, https://doi.org/10.1023/B:TOCA.0000013537.13540.0e.
[18] A.J.J.E. Eerhart, A.P.C. Faaij, M.K. Patel, Replacing fossil based PET with biobased PEF; process analysis, energy and GHG balance, Energy Environ. Sci. 5 (2012) 6407, https://doi.org/10.1039/c2ee02480b.
[19] M.G. Davidson, S. Elgie, S. Parsons, T.J. Young, Production of HMF, FDCA and their derived products: a review of life cycle assessment (LCA) and techno-economic analysis (TEA) studies, Green Chem. 23 (2021) 3154–3171, https://doi.org/10.1039/D1GC00721A.
[20] S.S. Sthal, P.L. Alsters, Liquid Phase Aerobic Oxidation Catalysis: Industrial Applications and Academic Perspectives, 1st ed., John Wiley & Sons, Ltd, 2016. DOI: 10.1002/9783527690121.
[21] M. Milić, P. Domínguez de María, S. Kara, A patent survey on the biotechnological production of 2,5-furandicarboxylic acid (FDCA): current trends and challenges, EFB Bioeconomy J. 3 (2023) 100050, https://doi.org/10.1016/j.bioeco.2023.100050.
[22] E. de Jong, H.A. Visser, A.S. Dias, C. Harvey, G.-J.-M. Gruter, The Road to Bring FDCA and PEF to the Market, Polymers 14 (5) (2022) 943.
[23] K.R. Vuyyuru, P. Strasser, Oxidation of biomass derived 5-hydroxymethylfurfural using heterogeneous and electrochemical catalysis, Catal. Today 195 (2012) 144–154, https://doi.org/10.1016/j.cattod.2012.05.008.
[24] D. Bonincontro, A. Lolli, A. Villa, L. Prati, N. Dimitratos, G.M. Veith, L. E. Chinchilla, G.A. Botton, F. Cavani, S. Albonetti, AuPd-nNiO as an effective catalyst for the base-free oxidation of HMF under mild reaction conditions, Green Chem. 21 (2019) 4090–4099, https://doi.org/10.1039/C9GC01283D.
[25] T. Pasini, M. Piccinini, M. Blosi, R. Bonelli, S. Albonetti, N. Dimitratos, J.A. Lopez-Sanchez, M. Sankar, Q. He, C.J. Kiely, G.J. Hutchings, F. Cavani, Selective oxidation of 5-hydroxymethyl-2-furfural using supported gold–copper nanoparticles, Green Chem. 13 (2011) 2091, https://doi.org/10.1039/c1gc15355b.
[26] C. Megías-Sayago, A. Lolli, D. Bonincontro, A. Penkova, S. Albonetti, F. Cavani, J. A. Odriozola, S. Ivanova, Effect of Gold Particles size over Au/C Catalyst Selectivity in HMF Oxidation Reaction, ChemCatChem 12 (2020) 1177–1183, https://doi.org/10.1002/cctc.201901742.
[27] W. Gong, K. Zheng, P. Ji, Platinum deposited on cerium coordination polymer for catalytic oxidation of hydroxymethylfurfural producing 2,5-furandicarboxylic acid, RSC Adv. 7 (2017) 34776–34782, https://doi.org/10.1039/C7RA05427K.
[28] B. Liu, Z. Zheng, Y. Liu, M. Zhang, Y. Wang, Y. Wan, K. Yan, Efficient electrooxidation of biomass-derived aldehydes over ultrathin NiV-layered double hydroxides films, J. Energy Chem. 78 (2023) 412–421, https://doi.org/10.1016/j.jechem.2022.11.041.
[29] W.-J. Liu, L. Dang, Z. Xu, H.-Q. Yu, S. Jin, G.W. Huber, Electrochemical Oxidation of 5-Hydroxymethylfurfural with NiFe Layered double Hydroxide (LDH) Nanosheet Catalysts, ACS Catal. 8 (2018) 5533–5541, https://doi.org/10.1021/acscatal.8b01017.
[30] K. Hu, M. Zhang, B. Liu, Z. Yang, R. Li, K. Yan, Efficient electrochemical oxidation of 5-hydroxymethylfurfural to 2,5-furandicarboxylic acid using the facilely synthesized 3D porous WO3/Ni electrode, Mol. Catal. 504 (2021) 111459, https://doi.org/10.1016/j.mcat.2021.111459.
[31] Y. Yang, T. Mu, Electrochemical oxidation of biomass derived 5-hydroxymethylfurfural (HMF): pathway, mechanism, catalysts and coupling reactions, Green Chem. 23 (2021) 4228–4254, https://doi.org/10.1039/D1GC00914A.
[32] A. Allegri, V. Maslova, M. Blosi, A.L. Costa, S. Ortelli, F. Basile, S. Albonetti, Photocatalytic Oxidation of HMF under Solar Irradiation: coupling of Microemulsion and Lyophilization to Obtain innovative TiO2-based Materials, Molecules 25 (2020) 5225, https://doi.org/10.3390/molecules25225225.
[33] M.A. do Nascimento, B. Haber, M.R.B.P. Gomez, R.A.C. Leão, M. Pietrowski, M. Zieliński, R.O.M.A. de Souza, R. Wojcieszak, I. Itabaiana, Optimization of 5-hydroxymethylfurfural oxidation via photo-enzymatic cascade process, Green Chem. (2024). DOI: 10.1039/D4GC00673A.
[34] Y. Zhang, G. Jia, W. Wang, L. Jiang, Z. Guo, Photocatalytic upgrading of 5-hydroxymethylfurfural – aerobic or anaerobic? Green Chem. 26 (2024) 2949–2966, https://doi.org/10.1039/D3GC04814D.
[35] S. Albonetti, A. Lolli, V. Morandi, A. Migliori, C. Lucarelli, F. Cavani, Conversion of 5-hydroxymethylfurfural to 2,5-furandicarboxylic acid over Au-based catalysts: optimization of active phase and metal–support interaction, Appl. Catal. B Environ. 163 (2015) 520–530, https://doi.org/10.1016/j.apcatb.2014.08.026.
[36] S. Albonetti, T. Pasini, A. Lolli, M. Blosi, M. Piccinini, N. Dimitratos, J.A. Lopez-Sanchez, D.J. Morgan, A.F. Carley, G.J. Hutchings, F. Cavani, Selective oxidation of 5-hydroxymethyl-2-furfural over TiO2-supported gold–copper catalysts prepared from preformed nanoparticles: effect of Au/Cu ratio, Catal. Today 195 (2012) 120–126, https://doi.org/10.1016/j.cattod.2012.05.039.
[37] C. Megías-Sayago, A. Lolli, S. Ivanova, S. Albonetti, F. Cavani, J.A. Odriozola, Au/Al2O3 – Efficient catalyst for 5-hydroxymethylfurfural oxidation to 2,5-furandicarboxylic acid, Catal. Today 333 (2019) 169–175, https://doi.org/10.1016/j.cattod.2018.04.024.
[38] C. Megías-Sayago, D. Bonincontro, A. Lolli, S. Ivanova, S. Albonetti, F. Cavani, J. A. Odriozola, 5-Hydroxymethyl-2-Furfural Oxidation over Au/CexZr1-xO2 Catalysts, accessed April 24, 2023, Front. Chem. 8 (2020), https://www.frontiersin.org/articles/10.3389/fchem.2020.00461.
[39] S.E. Davis, L.R. Houk, E.C. Tamargo, A.K. Datye, R.J. Davis, Oxidation of 5-hydroxymethylfurfural over supported Pt, Pd and Au catalysts, Catal. Today 160 (2011) 55–60, https://doi.org/10.1016/j.cattod.2010.06.004.
[40] Y.Y. Gorbanev, S.K. Klitgaard, J.M. Woodley, C.H. Christensen, A. Riisager, Gold-Catalyzed Aerobic Oxidation of 5-Hydroxymethylfurfural in Water at Ambient Temperature, ChemSusChem 2 (2009) 672–675, https://doi.org/10.1002/cssc.200900059.
[41] O. Casanova, S. Iborra, A. Corma, Biomass into Chemicals: Aerobic Oxidation of 5-Hydroxymethyl-2-furfural into 2,5-Furandicarboxylic Acid with Gold Nanoparticle Catalysts, ChemSusChem 2 (2009) 1138–1144, https://doi.org/10.1002/cssc.200900137.
[42] S.E. Davis, B.N. Zope, R.J. Davis, On the mechanism of selective oxidation of 5-hydroxymethylfurfural to 2,5-furandicarboxylic acid over supported Pt and Au catalysts, Green Chem. 14 (2012) 143–147, https://doi.org/10.1039/C1GC16074E.
[43] S.E. Davis, A.D. Benavidez, R.W. Gosselink, J.H. Bitter, K.P. de Jong, A.K. Datye, R. J. Davis, Kinetics and mechanism of 5-hydroxymethylfurfural oxidation and their implications for catalyst development, J. Mol. Catal. Chem. 388–389 (2014) 123–132, https://doi.org/10.1016/j.molcata.2013.09.013.
[44] S.E. Davis, M.S. Ide, R.J. Davis, Selective oxidation of alcohols and aldehydes over supported metal nanoparticles, Green Chem. 15 (2013) 17–45, https://doi.org/10.1039/C2GC36441G.
[45] S.M. Rogers, C.R.A. Catlow, D. Gianolio, P.P. Wells, N. Dimitratos, Supported metal nanoparticles with tailored catalytic properties through sol-immobilisation: applications for the hydrogenation of nitrophenols, Faraday Discuss. 208 (2018) 443–454, https://doi.org/10.1039/C7FD00216E.
[46] A. Villa, D. Wang, G.M. Veith, F. Vindigni, L. Prati, Sol immobilization technique: a delicate balance between activity, selectivity and stability of gold catalysts, Catal. Sci. Technol. 3 (2013) 3036, https://doi.org/10.1039/c3cy00260h.

[47] G. Fritz, V. Schädler, N. Willenbacher, N.J. Wagner, Electrosteric Stabilization of Colloidal Dispersions, Langmuir 18 (2002) 6381–6390.
[48] S. Campisi, M. Schiavoni, C.E. Chan-Thaw, A. Villa, Untangling the Role of the Capping Agent in Nanocatalysis: recent advances and Perspectives, Catalysts 6 (2016) 185, https://doi.org/10.3390/catal6120185.
[49] L.M. Rossi, J.L. Fiorio, M.A.S. Garcia, C.P. Ferraz, The role and fate of capping ligands in colloidally prepared metal nanoparticle catalysts, Dalton Trans. 47 (2018) 5889–5915, https://doi.org/10.1039/C7DT04728B.
[50] N. Yang, S. Pattisson, M. Douthwaite, G. Zeng, H. Zhang, J. Ma, G.J. Hutchings, Influence of Stabilizers on the Performance of Au/TiO $_2$ Catalysts for CO Oxidation, ACS Catal. 11 (2021) 11607–11615, https://doi.org/10.1021/acscatal.1c02820.
[51] P. Zhang, T.K. Sham, Tuning the electronic behavior of Au nanoparticles with capping molecules, Appl. Phys. Lett. 81 (2002) 736–738, https://doi.org/10.1063/1.1494120.
[52] H. Tsunoyama, N. Ichikuni, H. Sakurai, T. Tsukuda, Effect of Electronic Structures of Au Clusters Stabilized by Poly(N-vinyl-2-pyrrolidone) on Aerobic Oxidation Catalysis, J. Am. Chem. Soc. 131 (2009) 7086–7093, https://doi.org/10.1021/ja810045y.
[53] F. Liuzzi, A. Ventimiglia, A. Allegri, E. Rodríguez-Aguado, J.A. Cecilia, I. Rivalta, N. Dimitratos, S. Albonetti, Effect of Capping Ligands for the Synthesis of Gold Nanoparticles and on the Catalytic Performance for the Oxidation of 5-Hydroxymethyl-2-furfural, Catalysts 13 (2023) 990, https://doi.org/10.3390/catal13060990.
[54] S. Scurti, A. Allegri, F. Liuzzi, E. Rodríguez-Aguado, J.A. Cecilia, S. Albonetti, D. Caretti, N. Dimitratos, Temperature-Dependent activity of Gold Nanocatalysts Supported on Activated Carbon in Redox Catalytic Reactions: 5-Hydroxymethyl-furfural Oxidation and 4-Nitrophenol Reduction Comparison, Catalysts 12 (2022) 323, https://doi.org/10.3390/catal12030323.
[55] S. Scurti, E. Monti, E. Rodríguez-Aguado, D. Caretti, J.A. Cecilia, N. Dimitratos, Effect of polyvinyl Alcohol Ligands on Supported Gold Nano-Catalysts: Morphological and Kinetics Studies, Nanomaterials 11 (2021) 879, https://doi.org/10.3390/nano11040879.
[56] E. Monti, A. Ventimiglia, L. Forster, E. Rodríguez-Aguado, J.A. Cecilia, F. Ospitali, T. Tabanelli, S. Albonetti, F. Cavani, I. Rivalta, C. D'Agostino, N. Dimitratos, Influence of stabilisers on the catalytic activity of supported Au colloidal nanoparticles for the liquid phase oxidation of glucose to glucaric acid: understanding the catalyst performance from NMR relaxation and computational studies, Green Chem. (2023), https://doi.org/10.1039/D2GC04418H.
[57] O. Kwon, S. Barlow, S.A. Odom, L. Beverina, N.J. Thompson, E. Zojer, J.-L. Brédas, S.R. Marder, Aromatic Amines: a Comparison of Electron-Donor Strengths, J. Phys. Chem. A 109 (2005) 9346–9352, https://doi.org/10.1021/jp054334s.
[58] H. Häkkinen, M. Moseler, O. Kostko, N. Morgner, M.A. Hoffmann, B. v. Issendorff, Symmetry and Electronic Structure of Noble-Metal Nanoparticles and the Role of Relativity, Phys. Rev. Lett. 93 (2004) 093401. DOI: 10.1103/PhysRevLett.93.093401.
[59] M. Van Den Bossche, DFTB-Assisted Global Structure Optimization of 13- and 55-Atom late transition Metal Clusters, J. Phys. Chem. A 123 (2019) 3038–3045, https://doi.org/10.1021/acs.jpca.9b00927.
[60] A.D. Beeke, Density-functional thermochemistry. III. the role of exact exchange, J. Chem. Phys. 98 (1993) 5648–5652.
[61] B. Helmich-Paris, B. de Souza, F. Neese, R. Izsák, An improved chain of spheres for exchange algorithm, J. Chem. Phys. 155 (2021) 104109, https://doi.org/10.1063/5.0058766.
[62] F. Weigend, Accurate Coulomb-fitting basis sets for H to Rn, Phys. Chem. Chem. Phys. 8 (2006) 1057–1065, https://doi.org/10.1039/B515623H.
[63] V. Barone, M. Cossi, Quantum Calculation of Molecular Energies and Energy Gradients in solution by a Conductor Solvent Model, J. Phys. Chem. A 102 (1998) 1995–2001, https://doi.org/10.1021/jp9716997.
[64] S. Grimme, S. Ehrlich, L. Goerigk, Effect of the damping function in dispersion corrected density functional theory, J. Comput. Chem. 32 (2011) 1456–1465, https://doi.org/10.1002/jcc.21759.
[65] F. Neese, F. Wennmohs, U. Becker, C. Riplinger, The ORCA quantum chemistry program package, J. Chem. Phys. 152 (2020) 224108, https://doi.org/10.1063/5.0004608.
[66] P.J. Hay, W.R. Wadt, Ab initio effective core potentials for molecular calculations. Potentials for the transition metal atoms Sc to Hg, J. Chem. Phys. 82 (1985) 270–283, https://doi.org/10.1063/1.448799.
[67] T. Lu, F. Chen, Atomic dipole moment corrected hirshfeld population method, J. Theor. Comput. Chem. 11 (2012) 163–183, https://doi.org/10.1142/S0219633612500113.
[68] B.H. Besler, K.M. Merz Jr., P.A. Kollman, Atomic charges derived from semiempirical methods, J. Comput. Chem. 11 (1990) 431–439, https://doi.org/10.1002/jcc.540110404.
[69] T. Lu, F. Chen, Multiwfn: a multifunctional wavefunction analyzer, J. Comput. Chem. 33 (2012) 580–592, https://doi.org/10.1002/jcc.22885.
[70] E. Fukushima, S.B. Roeder, Experimental pulse NMR: a nuts and bolts approach, Westview Press, Boulder, Clorado, 2016.
[71] H.Y. Carr, E.M. Purcell, Effects of Diffusion on Free Precession in Nuclear magnetic Resonance Experiments, Phys. Rev. 94 (1954) 630–638, https://doi.org/10.1103/PhysRev.94.630.
[72] A. Heuer-Jungemann, N. Feliu, I. Bakaimi, M. Hamaly, A. Alkilany, I. Chakraborty, A. Masood, M.F. Casula, A. Kostopoulou, E. Oh, K. Susumu, M.H. Stewart, I. L. Medintz, E. Stratakis, W.J. Parak, A.G. Kanaras, The Role of Ligands in the Chemical Synthesis and applications of Inorganic Nanoparticles, Chem. Rev. 119 (2019) 4819–4880, https://doi.org/10.1021/acs.chemrev.8b00733.
[73] Y. Lyu, L.M. Becerril, M. Vanzan, S. Corni, M. Cattelan, G. Granozzi, M. Frasconi, P. Rajak, P. Banerjee, R. Ciancio, F. Mancin, P. Scrimin, The Interaction of Amines with Gold Nanoparticles, Adv. Mater. n/a (n.d.) 2211624. DOI: 10.1002/adma.202211624.
[74] R.G. Pearson, Hard and soft acids and bases, HSAB, part 1: fundamental principles, J. Chem. Educ. 45 (1968) 581, https://doi.org/10.1021/ed045p581.
[75] L.-H. Lee, Application of Hard-Soft Acid-Base (HSAB) Principle to Solid Adhesion and Surface Interactions Between Metals and Polymers, in: L.-H. Lee (Ed.), New Trends Phys. Physucal Chem. Polym., Springer US, Boston, MA, 1989: pp. 185–196. DOI: 10.1007/978-1-4613-0543-9_15.
[76] J. Pritchard, L. Kesavan, M. Piccinini, Q. He, R. Tiruvalam, N. Dimitratos, J. A. Lopez-Sanchez, A.F. Carley, J.K. Edwards, C.J. Kiely, G.J. Hutchings, Direct Synthesis of Hydrogen Peroxide and Benzyl Alcohol Oxidation using Au−Pd Catalysts Prepared by Sol Immobilization, Langmuir 26 (2010) 16568–16577, https://doi.org/10.1021/la101597q.
[77] Y. Wu, P. Jiang, M. Jiang, T.-W. Wang, C.-F. Guo, S.-S. Xie, Z.-L. Wang, The shape evolution of gold seeds and gold@silver core-shell nanostructures, Nanotechnology 20 (2009) 305602, https://doi.org/10.1088/0957-4484/20/30/305602.
[78] A. Patnaik, C. Li, Evidence for metal interaction in gold metallized polycarbonate films: an x-ray photoelectron spectroscopy investigation, J. Appl. Phys. 83 (1998) 3049–3056, https://doi.org/10.1063/1.367059.
[79] S. Scurti, G.P. Salanitri, T. Mecca, E. Rodríguez-Aguado, J.A. Cecilia, G. Curcuruto, S.C. Carroccio, D. Caretti, N. Dimitratos, pH-dependent catalytic activity of Au and Pd-based hybrid cryogels by investigating the acid/base nature of the polymeric phase, Mater. Today Chem. 38 (2024) 102046, https://doi.org/10.1016/j.mtchem.2024.102046.
[80] R.P. Herrera, M.C. Gimeno, Main Avenues in Gold Coordination Chemistry, Chem. Rev. 121 (2021) 8311–8363, https://doi.org/10.1021/acs.chemrev.0c00930.
[81] H. Goodman, L. Mei, T.L. Gianetti, Molecular Orbital Insights of transition Metal-Stabilized Carbocations, Front. Chem. 7 (2019) 365, https://doi.org/10.3389/fchem.2019.00365.
[82] P. Tripathy, A. Mishra, S. Ram, H.-J. Fecht, J. Bansmann, R.J. Behm, X-ray photoelectron spectrum in surface interfacing of gold nanoparticles with polymer molecules in a hybrid nanocomposite structure, Nanotechnology 20 (2009) 075701, https://doi.org/10.1088/0957-4484/20/7/075701.
[83] M. Kobayashi, A. Takahara, Tribological properties of hydrophilic polymer brushes under wet conditions, Chem. Rec. 10 (2010) 208–216, https://doi.org/10.1002/tcr.201000001.
[84] C. D'Agostino, J. Mitchell, M.D. Mantle, L.F. Gladden, Interpretation of NMR Relaxation as a Tool for Characterising the Adsorption Strength of Liquids inside Porous Materials, Chem. – Eur. J. 20 (2014) 13009–13015, https://doi.org/10.1002/chem.201403139.
[85] C. D'Agostino, Y. Ryabenkova, P.J. Miedziak, S.H. Taylor, G.J. Hutchings, L. F. Gladden, M.D. Mantle, Deactivation studies of a carbon supported AuPt nanoparticulate catalyst in the liquid-phase aerobic oxidation of 1,2-propanediol, Catal, Sci. Technol. 4 (2014) 1313–1322, https://doi.org/10.1039/C4CY00027G.
[86] G. Filippini, F. Longobardo, L. Forster, A. Criado, G. Di Carmine, L. Nasi, C. D'Agostino, M. Melchionna, P. Fornasiero, M. Prato, Light-driven, heterogeneous organocatalysts for C–C bond formation toward valuable perfluoroalkylated intermediates, Sci. Adv. 6 (2020) eabc9923, https://doi.org/10.1126/sciadv.abc9923.
[87] H. Ait Rass, N. Essayem, M. Besson, Selective Aerobic Oxidation of 5-HMF into 2,5-Furandicarboxylic Acid with Pt Catalysts Supported on TiO $_2$ - and ZrO $_2$ -based Supports, ChemSusChem 8 (2015) 1206–1217, https://doi.org/10.1002/cssc.201403390.
[88] S. Liu, Y. Zhu, Y. Liao, H. Wang, Q. Liu, L. Ma, C. Wang, Advances in understanding the humins: formation, prevention and applicatio, Appl. Energy Combust. Sci. 10 (2022) 100062, https://doi.org/10.1016/j.jaecs.2022.100062.
[89] A. Lolli, S. Albonetti, L. Utili, R. Amadori, F. Ospitali, C. Lucarelli, F. Cavani, Insights into the reaction mechanism for 5-hydroxymethylfurfural oxidation to FDCA on bimetallic Pd–Au nanoparticles, Appl. Catal. Gen. 504 (2015) 408–419, https://doi.org/10.1016/j.apcata.2014.11.020.
[90] G.F. Tierney, S. Alijani, M. Panchal, D. Decarolis, M.B. de Gutierrez, K.M. H. Mohammed, J. Callison, E.K. Gibson, P.B.J. Thompson, P. Collier, N. Dimitratos, E.C. Corbos, F. Pelletier, A. Villa, P.P. Wells, Controlling the production of Acid Catalyzed Products of Furfural Hydrogenation by Pd/TiO2, ChemCatChem 13 (2021) 5121–5133, https://doi.org/10.1002/cctc.202101036.
[91] Y. Zhao, L. Jia, J.A. Medrano, J.R.H. Ross, L. Lefferts, Supported Pd Catalysts Prepared via Colloidal Method: the effect of Acids, ACS Catal. 3 (2013) 2341–2352, https://doi.org/10.1021/cs4004479.